Cell Metabolism
Short Article

Resistance of Ferroportin to Hepcidin Binding causes Exocrine Pancreatic Failure and Fatal Iron Overload

Sandro Altamura,[1,2] Regina Kessler,[1,2] Hermann-Josef Gröne,[3] Norbert Gretz,[4] Matthias W. Hentze,[2,5,6] Bruno Galy,[5,6,*] and Martina U. Muckenthaler[1,2,6,*]
[1]Department of Pediatric Hematology, Oncology and Immunology, University of Heidelberg, INF 350, 69120 Heidelberg, Germany
[2]Molecular Medicine Partnership Unit, 69120 Heidelberg, Germany
[3]Deutsches Krebsforschungszentrum, 69120 Heidelberg, Germany
[4]Medical Faculty Mannheim, 68167 Mannheim, Germany
[5]European Molecular Biology Laboratory, 69120 Heidelberg, Germany
[6]Co-senior author
*Correspondence: galy@embl.de (B.G.), martina.muckenthaler@med.uni-heidelberg.de (M.U.M.)
http://dx.doi.org/10.1016/j.cmet.2014.07.007

SUMMARY

The regulatory axis between the iron hormone hepcidin and its receptor, the iron exporter ferroportin (FPN), is central to iron homeostasis. Mutations preventing hepcidin-mediated degradation of FPN cause systemic iron overload. We have introduced a point mutation (C326S) into the murine *Fpn* locus, resembling human hereditary hemochromatosis type 4, including elevated plasma iron and ferritin levels, high transferrin saturation, hepatic iron overload, and iron depletion of duodenal enterocytes and reticuloendothelial macrophages. Unlike other mouse models of iron overload, homozygous C326S mice die between 7 and 14 months of age. Pancreatic acinar cells display marked iron accumulation, oxidative damage and degeneration, associated with failure of the exocrine pancreas and severe body weight loss. Rescue experiments reveal iron overload and exocrine pancreatic failure as leading causes of death. This work uncovers the critical importance of the hepcidin-ferroportin regulatory axis for life and unveils the sensitivity of the exocrine pancreas to iron overload.

INTRODUCTION

The hepcidin-ferroportin (FPN) regulatory circuitry evolved in vertebrates to maintain physiological systemic iron levels (Hentze et al., 2010). Hepcidin is a small peptide hormone secreted by the liver in response to increased systemic iron levels or inflammatory cytokines. It binds to FPN, its only known receptor (Nemeth et al., 2004). FPN is encoded by the *SLC40A1* gene, a multipass transmembrane protein that exports iron primarily from duodenal enterocytes, reticuloendothelial macrophages, or placental syncytiotrophoblasts into the bloodstream (Donovan et al., 2005; McKie et al., 2000). Hepcidin binds to the fourth extracellular loop of FPN to trigger its ubiquitinylation on multiple lysine residues located in the third intracellular domain (Qiao et al., 2012). This causes ferroportin internalization and degradation in lysosomes. Low FPN expression reduces iron export into the plasma, thus retaining iron in FPN-expressing cells and lowering systemic iron availability (Nemeth et al., 2004).

Human ferroportin disease is an inherited iron overload disorder hallmarked by either loss-of-function mutations that impair the capacity of FPN to export iron or gain-of-function mutations that prevent hepcidin-mediated FPN control (Pietrangelo, 2004). Gain-of-function mutations cause hereditary hemochromatosis type 4 (HH type 4) with elevated transferrin saturation, hyperferritinemia, and tissue iron overload (Pietrangelo, 2004). In 2005, a case of HH type 4 caused by substitution of cysteine 326 for a serine in the FPN protein was reported (Sham et al., 2005). Functional studies in cellular models suggested the critical importance of C326 for hepcidin binding (Fernandes et al., 2009). Here, we report the generation of the first mouse model of HH type 4 due to resistance to hepcidin. In this disease model, the endogenous ferroportin locus was mutagenized to introduce the C326S mutation. We demonstrate that the C326S mutation suffices to cause resistance to hepcidin binding in vivo. A thorough characterization of C326S mutant mice reveals that the hepcidin-FPN interaction is essential to prevent fatal iron overload. Our study also uncovers the importance of the hepcidin-FPN regulatory axis for proper function of the exocrine pancreas.

RESULTS AND DISCUSSION

Generation of the *Slc40a1*^{C326S} Knockin Mice

We targeted the *Slc40a1* locus of mouse embryonic stem cells (ESCs) using a construct containing the C326S point mutation in the seventh *Fpn* exon together with an intronic, floxed, promoterless β-*Geo* selection marker. Insertion of the β-*Geo* cassette into the sixth intron of the *Slc40a1* locus results in a trapped allele (*Slc40a1*^{trap}) expressing a chimeric, bicistronic mRNA from the endogenous *Slc40a1* promoter that comprises the first six *Fpn* exons fused to the β-Geo marker. The *Slc40a1*^{trap} mouse line was obtained through injection of targeted ESCs into mouse blastocysts, followed by germline transmission of the targeted allele. Southern blot analysis confirmed the proper and unique targeting of the *Slc40a1* locus (Figures 1A and 1B). To obtain the C326S

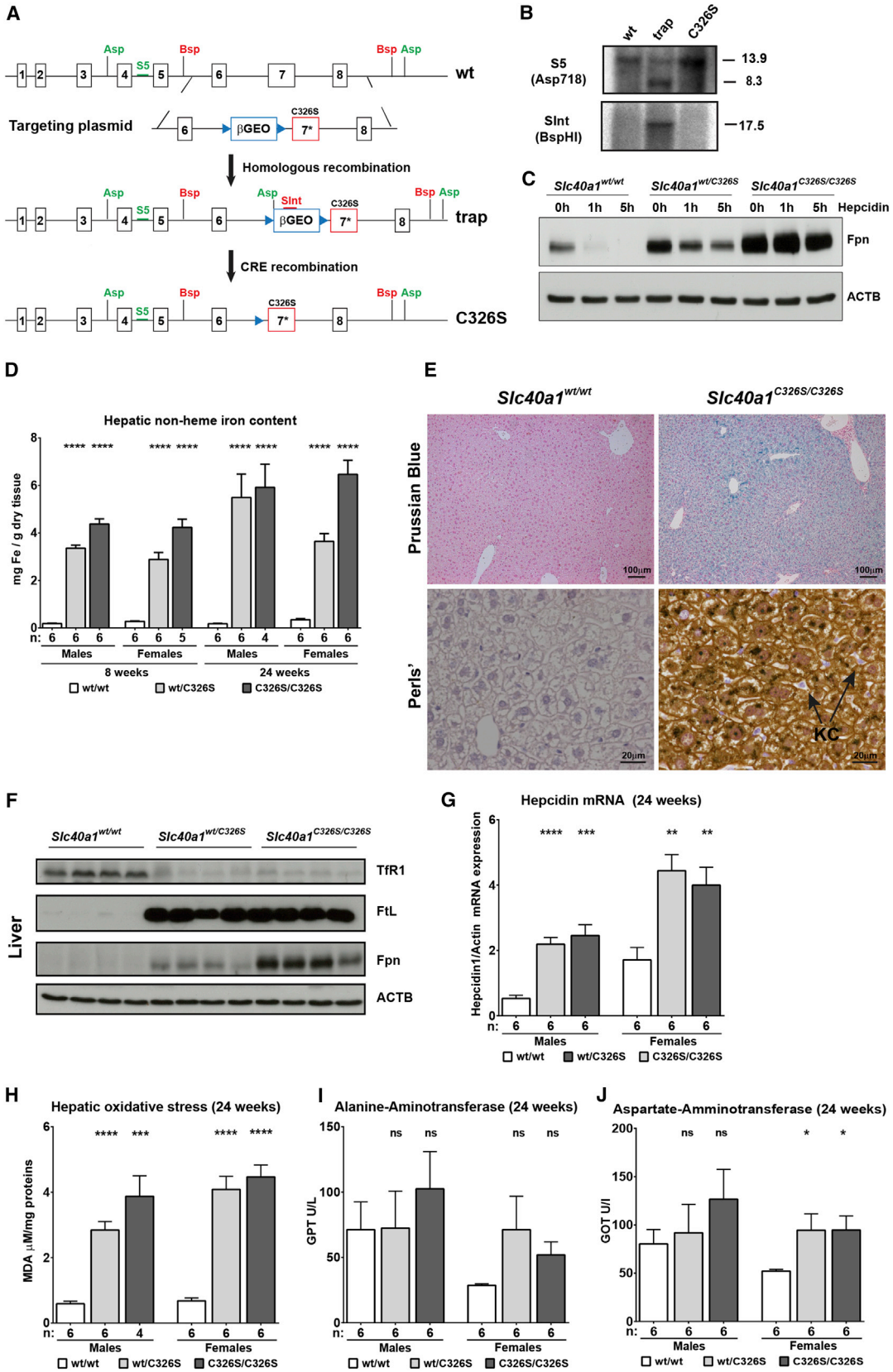

(legend on next page)

knockin strain (*Slc40a1*^{C326S}), the floxed β-*Geo* cassette was removed by crossing the *Slc40a1*^{trap} line to a CRE-deletor strain expressing CRE recombinase under the control of the constitutively active *Hprt* promoter (Tang et al., 2002). CRE-mediated deletion of the β-*Geo* cassette restores the normal ferroportin splicing pattern and produces a mRNA that differs from wild-type by a single point mutation introducing the C326S amino acid substitution (Figure 1A). Effective excision of the β-Geo sequence was ascertained by Southern blotting (Figure 1B).

Heterozygous *Slc40a1*$^{wt/C326S}$ mice were intercrossed to generate homozygous mutant (*Slc40a1*$^{C326S/C326S}$) and wild-type littermates. The *Slc40a1*^{C326S} allele is inherited in Mendelian proportions, in both male and female mice (Table S1). *Slc40a1*$^{C326S/C326S}$ mice are phenotypically indistinguishable from wild-type littermates at birth and reach adulthood without overt abnormalities: 8- to 10-week-old animals maintained on a standard rodent diet exhibit an overall healthy phenotype, are fertile, have a normal body weight, and display normal posture and behavior without evidence of neurological or muscular impairment (data not shown).

To assess whether the C326S mutation confers the predicted resistance to hepcidin, bone marrow-derived macrophages (BMDMs) from 10-week-old wild-type, heterozygous *Slc40a1*$^{wt/C326S}$, and homozygous *Slc40a1*$^{C326S/C326S}$ mice were either left untreated or exposed to synthetic hepcidin (1 μg/ml) for 1–5 hr, and FPN protein expression was analyzed by western blotting (Figure 1C). In wild-type BMDMs, FPN expression is markedly suppressed after 1 hr exposure to hepcidin and is no longer detected after 5 hr of treatment. Importantly, FPN suppression by hepcidin is strongly impaired in BMDMs from *Slc40a1*$^{wt/C326S}$ mice and completely abolished in *Slc40a1*$^{C326S/C326S}$ cells, at least during the time course of the experiment. Note that basal FPN levels are higher in *Slc40a1*$^{wt/C326S}$ and *Slc40a1*$^{C326S/C326S}$ than in wild-type cells, most likely reflecting the presence of residual amounts of hepcidin in the culture medium and/or endogenous production of hepcidin by BMDMs. Altogether, these results show that we have created a mouse line with bona fide FPN resistance of hepcidin.

Slc40a1^{C326S} Mice Mimic Hereditary Hemochromatosis Type 4

A patient reported to bear a heterozygous *FPN* C326S mutation suffers from juvenile HH characterized by severe hyperferremia and hyperferritinemia (Sham et al., 2005). Young adult SLC40A1$^{wt/C326S}$ and SLC40A1$^{C326S/C326S}$ mice exhibit the major hallmarks of HH type 4, with high transferrin saturation and a marked increase in serum ferritin levels (Table 1). Consistent with earlier studies of HH patients (McLaren et al., 2007), *Slc40a1*$^{C326S/C326S}$ animals also show elevated red blood cell counts associated with high hemoglobin and hematocrit values and enlarged mean corpuscular volume (MCV) (Table 1). The murine C326S mutation thus recapitulates the iron overload pattern of the same mutation and of other gain-of-function mutations in the human ferroportin gene. *Fpn* is transcriptionally regulated by zinc and copper (Chung et al., 2004; Troadec et al., 2010), and the protein can export zinc in cellular assays (Troadec et al., 2010). Inductively coupled plasma mass spectrometry (ICP/MS) analysis in the plasma of *Slc40a1*$^{C326S/C326S}$ mice did not show changes in the amount of zinc and copper (Table S2). Sodium, calcium, and phosphate levels were also unaffected (Table S2). Hence, FPN resistance to hepcidin and the ensuing increase in FPN levels (see below) do not impact metal homeostasis in general, but they specifically alter iron metabolism.

Hepatic Phenotype of Hepcidin-Resistant Animals

Iron deposition in the liver of untreated HH patients causes progressive hepatic damage and increases the risk of cirrhosis and hepatocellular carcinoma (Pietrangelo, 2010). Compared to wild-type, *Slc40a1*$^{wt/C326S}$ and *Slc40a1*$^{C326S/C326S}$ mice display a dramatic increase in hepatic iron levels, regardless of gender (Figure 1D). Prussian blue staining reveals preferential iron deposition in the pericentral areas of the liver lobules (Figure 1E, top), which is associated with reduced FPN expression in this area (Figure S1C, available online). Perls' staining shows that iron accumulates exclusively in hepatocytes (Figure 1E, bottom). Kupffer cells, specialized iron-exporting macrophages located in hepatic sinusoids, are iron spared (Figure 1E, bottom); this is consistent with the C326S form of FPN being constitutively overexpressed in macrophages (Figure S1C) and exporting iron into the bloodstream in an uncontrolled manner.

Hepatic iron loading downregulates transferrin receptor 1 (TfR1) (Figures 1F and S1A) and stimulates expression of the iron storage protein ferritin light chain (FtL) (Figure 1F). These effects likely reflect iron regulatory protein/iron responsive element (IRP/IRE)-dependent regulation of TFR1 and FtL in hepatocytes (Hentze and Kühn, 1996). C326S mutant mice also overexpress FPN compared to wild-type, with the highest expression in *Slc40a1*$^{C326S/C326S}$ animals and intermediate

Figure 1. Generation of C326S-FPN Mutant Mice and Analyses of BMDM and Liver

(A) Schematic representation of the *Slc40a1* wild-type (WT), targeted (trap), and C326S loci together with the targeting construct. The β-*Geo* cassette is flanked with *LoxP* sites (blue triangles); the mutated exon 7 bearing the C326S substitution (indicated with 7*) is represented in red. The 5′ external probe (S5) and the β-*Geo* internal probe (SInt) are shown. The Asp718 (Asp) and BspHI (Bsp) restriction sites are indicated.

(B) *Slc40a1* wild-type (WT), targeted (trap), and C326S alleles were analyzed by Southern blotting using the indicated restriction enzymes and probes.

(C) BMDMs from wild-type, *Slc40a1*$^{wt/C326S}$, and *Slc40a1*$^{C326S/C326S}$ mice were incubated with synthetic hepcidin for the time indicated and subjected to western blot against FPN; β-actin (ACTB) was used as loading control.

(D) The hepatic nonheme iron content was determined in 8- and 24-week-old mice.

(E) Prussian blue and Perls' staining of liver sections from 24-week-old *Slc40a1*$^{wt/wt}$ and *Slc40a1*$^{C326S/C326S}$ male mice. KC, Kupffer cells.

(F) Western blot analysis of TfR1, ferritin light chain (FTL), and FPN expression in the liver of *Slc40a1*$^{wt/wt}$, *Slc40a1*$^{wt/C326S}$, and *Slc40a1*$^{C326S/C326S}$ mice at 24 weeks of age. β-actin (ACTB) detection ascertained equal sample loading.

(G) Hepatic hepcidin mRNA expression was determined by quantitative RT-PCR (qRT-PCR) and calibrated to β-actin mRNA levels.

(H) Hepatic oxidative stress was measured as lipid peroxidation with the TBARS assay and normalized against total protein amount.

(I and J) Analysis of transaminases (GPT [I] and GOT [J]) in the plasma of 24-week-old animals.

Data are reported as mean ± SEM. Student's t test: *$p < 0.05$; **$p < 0.01$; ***$p < 0.001$; ****$p < 0.0001$. See also Figure S1 and Table S1.

Table 1. Plasma Iron Levels and Hematological Parameters in 10-Week-Old Mice

	Males						Females					
Parameter	WT/WT	n	WT/C326S	n	C326S/C326S	n	WT/WT	n	WT/C326S	n	C326S/C326S	n
Plasma Fe (μg/dl)	129.7 ± 7.8	6	353.5 ± 12.1****	5	350.7 ± 5.1****	6	166.4 ± 3.8	6	330.4 ± 12.4****	6	332.1 ± 10.2****	5
UIBC (μg/dl)	178.9 ± 6.7	6	42.6 ± 7.8****	5	37.6 ± 8.5****	6	179.5 ± 5.6	6	28.1 ± 2.1****	6	18.4 ± 4.5****	5
TfSat (%)	42.0 ± 2.1	6	89.4 ± 1.7****	5	90.6 ± 1.8****	6	48.1 ± 1.1	6	92.1 ± 0.7****	6	94.8 ± 1.2****	5
Ferritin (ng/ml)	137.9 ± 17.4	6	684.2 ± 123.3***	4	1,748 ± 524*	6	189 ± 10.5	6	735.5 ± 123.6**	6	739.4 ± 124.0***	5
RBC (10^{12}/l)	9.78 ± 0.09	12	10.23 ± 0.07***	12	10.33 ± 0.16**	10	10.00 ± 0.10	11	10.04 ± 0.19	12	10.15 ± 0.04	7
Hb (g/dl)	15.71 ± 0.15	12	16.91 ± 0.15****	12	17.19 ± 0.13****	10	16.13 ± 0.15	11	16.79 ± 0.23*	12	16.74 ± 0.25*	7
Hct (%)	50.7 ± 0.6	12	55.1 ± 0.4****	12	55.3 ± 0.8****	10	52.1 ± 0.5	11	53.6 ± 1.0	12	53.9 ± 0.2*	7
MCV (fl)	51.8 ± 0.3	12	54.1 ± 0.2****	12	53.6 ± 0.4**	10	52.1 ± 0.2	11	53.3 ± 0.2***	12	53.3 ± 0.2**	7
MCH (pg)	16.1 ± 0.1	12	16.5 ± 0.1**	12	16.7 ± 0.1	10	16.1 ± 0.1	11	16.8 ± 0.2**	12	16.5 ± 0.2	7
MCHC (g/dl)	30.99 ± 0.15	12	30.68 ± 0.13	12	31.10 ± 0.43	10	30.98 ± 0.18	11	31.40 ± 0.33	12	31.03 ± 0.38	7

UIBC, unsaturated iron binding capacity; TfSat, transferrin saturation; RBC, red blood cell; Hb, hemoglobin; Hct, hematocrit; MCV, mean corpuscular volume; MCH, mean corpuscular hemoglobin; MCHC, mean corpuscular hemoglobin concentration. Data are reported as mean ± SEM. Student's t test: *p < 0.05; **p < 0.01; ***p < 0.001; ****p < 0.0001. See also Table S2.

levels in heterozygotes (Figure 1F). This is most probably explained by decreased turnover of the hepcidin-insensitive FPN mutant protein (Figure S1C) but is also partly due to increased FPN transcript levels (Figure S1A); derepression of FPN translation by iron-mediated inhibition of the IRP/IRE system (McKie et al., 2000) may also contribute. Importantly, *Slc40a1*$^{wt/C326S}$ and *Slc40a1*$^{C326S/C326S}$ mice express levels of hepcidin mRNA in the liver significantly higher than those of wild-type (Figure 1G), associated with an increased expression of BMP6, ID1, SMAD6, and SMAD7 mRNAs (Figure S1A). These responses show that hepatocytes of C326S mutant mice adequately sense the iron overload and activate the BMP/SMAD signaling pathway with the concomitant expression of *Hepcidin*. Yet, the hepcidin response remains ineffective because the hormone fails to bind its receptor FPN. This phenotype is consistent with systemic and hepatic iron overload of patients with HH type 4 in spite of elevated hepcidin levels (Sham et al., 2009). These data also support the notion that hepcidin controls iron metabolism largely or exclusively through interaction with FPN.

Iron excess elicits its deleterious effects by promoting the generation of reactive oxygen species (ROS), which cause damage to proteins, DNA, and lipids (Altamura and Muckenthaler, 2009). Iron loading in the liver of 24-week-old *Slc40a1*$^{wt/C326S}$ and *Slc40a1*$^{C326S/C326S}$ animals is associated with marked lipid peroxidation, as evidenced by their substantial increase in thiobarbituric acid reactive substances (TBARS) (Figure 1H). Yet, blood levels of alanine transaminase remain within the normal range (Figure 1I), and aspartate transaminase is only mildly increased in female mice (Figure 1J). Furthermore, we observed no histological sign of liver damage (Figure S1B). These results show that hepatic iron loading in C326S mutant animals does not impair liver integrity and function (at least up to 24 weeks of age). These findings support the notion that mice, unlike patients, are protected from liver damage even in the context of severe tissue iron overload by as-yet-unknown mechanisms.

Unrestrained Iron Export from Macrophages and Enterocytes in C326S Mutant Mice

Splenic macrophages recycle iron from senescent red blood cells and export the metal into the bloodstream via FPN (Donovan et al., 2000). C326S FPN mutant mice exhibit decreased splenic iron levels at 8 and 24 weeks of age (Figure 2A). Perls' staining of spleen sections reveals selective iron depletion within iron-recycling macrophages of the red pulp (Figure 2B). Iron depletion of macrophages is further evidenced by decreased FtL expression in the spleen (Figure 2C, middle). These alterations are attributed to the constitutive, abnormally high expression of the FPN iron exporter (Figure 2C, top). FPN is overexpressed in spite of highly elevated *Hepcidin* expression (Figure 1G), again demonstrating that the C326S mutation renders FPN insensitive to hepcidin in vivo, as observed ex vivo in BMDMs (Figure 1C). Iron depletion of macrophages is predicted to activate iron regulatory proteins, inhibit ferritin translation (see above), and also repress the translation of FPN mRNA (McKie et al., 2000). If this occurs, the degree of repression is notably insufficient to prevent the overexpression of hepcidin-insensitive FPN, uncontrolled iron export from macrophages, and systemic iron overload, implying that the regulation of body iron recycling by hepcidin prevails. Notably, mice carrying either one or two copies of the C326S *Fpn* allele display similar levels of Fpn expression (Figure 2C) and similar levels of iron depletion in the spleen (Figure 2A). This suggests that the C326S mutation exerts a functionally dominant effect in splenic macrophages.

FPN is also expressed in duodenal enterocytes, where it mediates the transport of dietary iron into the bloodstream (McKie et al., 2000). Similar to the reticuloendothelial macrophages (Figures 2A and 2B), the intestinal epithelium of *Slc40a1*$^{C326S/C326S}$ animals is iron depleted compared to wild-type (Figure 2D, top). This iron depletion is associated with overexpression of the C326S FPN mutant protein (Figure 2E, middle) that accumulates at the basolateral side of enterocytes (Figure 2D, middle). FPN mRNA levels are also increased (Figure 2F), and thus both transcriptional (Taylor et al., 2011) and posttranslational regulatory mechanisms, due to the hepcidin resistance, appear to contribute to high FPN expression in the intestine of C326S mutant animals. The increased FPN expression is accompanied by an elevation of the iron uptake protein DMT1 (Figure 2E, top) at the apical membrane of enterocytes (Figure 2D, bottom). DMT1 expression is augmented at least in part at the mRNA level, as indicated by the DMT1-1A (Figure 2G) and -IRE

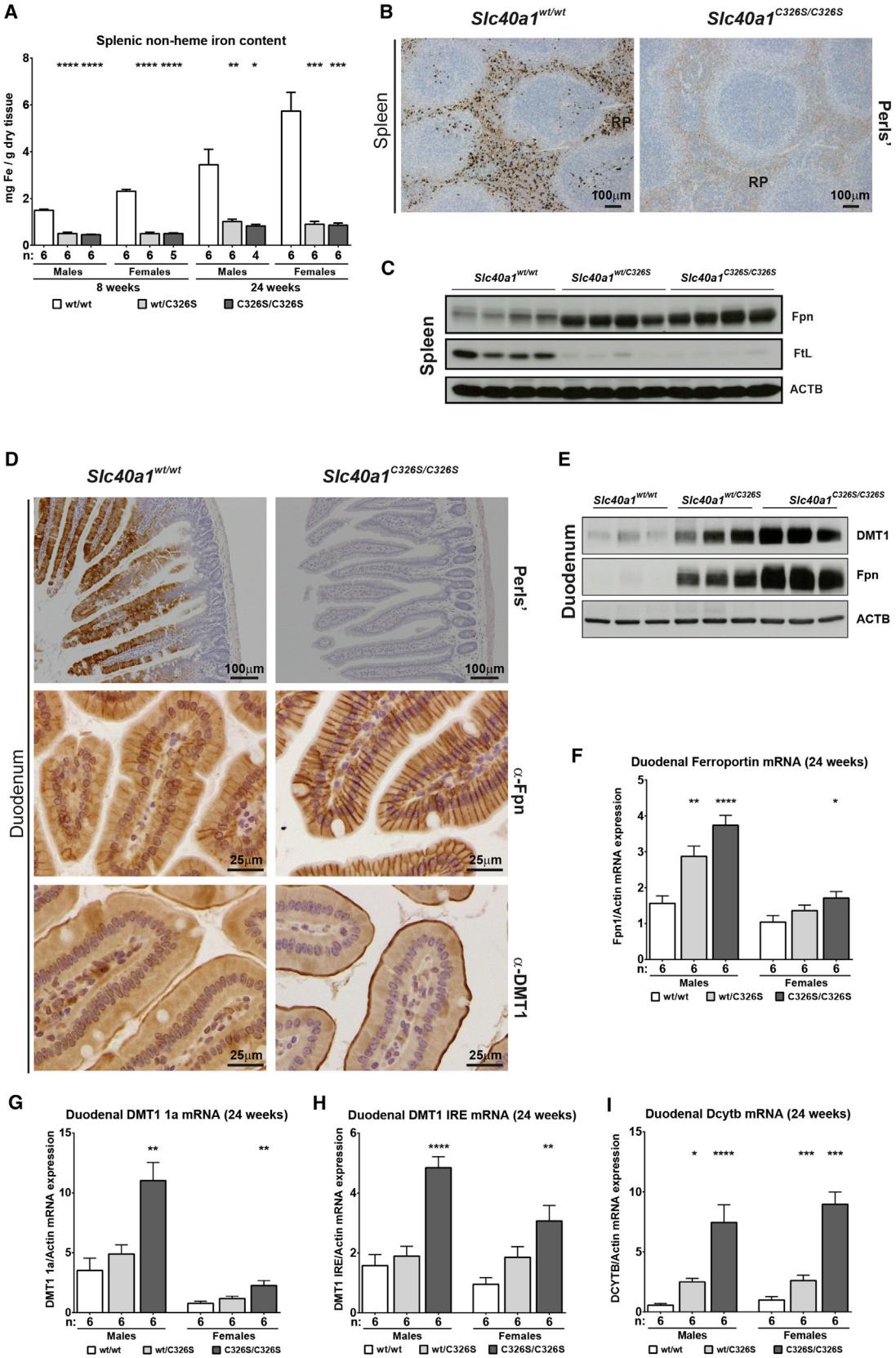

(legend on next page)

(Figure 2H) mRNA variants. DMT1 upregulation in adult C326S animals is likely unrelated to IRP control of DMT1 mRNA turnover (Galy et al., 2013) and most likely reflects stabilization of the HIF2α transcription factor in iron-depleted enterocytes and subsequent enhancement of *Dmt1* transcription (Mastrogiannaki et al., 2009). This notion is further supported by the increased expression of *Dcytb* ferric reductase (Figure 2I), another HIF2α target gene (Mastrogiannaki et al., 2009). Interestingly, DMT1 expression in enterocytes is augmented (Figures 2D and 2E) in spite of high hepcidin levels (Figure 1G). Hepcidin has been proposed to directly target DMT1 for degradation in enterocytes ex vivo (Brasse-Lagnel et al., 2011), but our data indicate that such a mechanism, if effective in vivo, fails to efficiently suppress the apical iron uptake machinery in the duodenum of C326S FPN mutant mice.

In contrast to the spleen (Figure 2C, top), duodenal enterocytes from *Slc40a1*$^{C326S/C326S}$ mice display a stronger increase in FPN protein levels compared to *Slc40a1*$^{wt/C326S}$ (Figure 2E, middle). This suggests that the C326S FPN mutation is not dominant in the intestine. Consequently, *Slc40a1*$^{C326S/C326S}$ mice may export more dietary iron into the blood stream than *Slc40a1*$^{wt/C326S}$ littermates, while the iron export capacity of macrophages seems the same. Differences in systemic iron accumulation between *Slc40a1*$^{wt/C326S}$ and *Slc40a1*$^{C326S/C326S}$ mice are not accounted for by differences in transferrin saturation (Table 1), which is close to 100% in both genotypes. Possibly, circulating nontransferrin bound iron (NTBI) may be increased in *Slc40a1*$^{C326S/C326S}$ mice. This is reflected on the organ level, whereby kidney (Figure S2A), heart (Figure S2B), pancreas (see below), and brain (Figure S2C) accumulate more iron in *Slc40a1*$^{C326S/C326S}$ than *Slc40a1*$^{wt/C326S}$ animals. Iron in the kidney accumulates predominantly in the renal medulla (Figure S2D), while in the heart the metal is detected mainly in vascular smooth muscle cells (Figure S2E). Accumulation of brain iron is detected in the choroid plexus (Figure S2F).

Taken together, the analyses of C326S FPN mutant mice yield insight into the hierarchy of iron regulatory mechanisms operational in iron-exporting cell types and uncover the dominant role of the FPN-hepcidin axis for systemic iron homeostasis in vivo.

Hepcidin Binding to FPN Is Critical for Exocrine Pancreatic Function and Organismal Survival

The necropsy of *Slc40a1*$^{C326S/C326S}$ mice revealed not only the expected dark brown coloration of the liver, but also dark brown coloration of the pancreas, suggestive of iron deposition (Figure 3A). Indeed, C326S FPN mutant mice show progressive and marked iron accumulation in the pancreatic tissue (Figure 3B). Consistently, TFR1 protein levels are decreased, while ferritin light (FtL) and heavy (FtH) chain expression is augmented (Figure 3F), as expected in iron overloaded cells. Similar to the liver (Figure 1H), iron accumulation in the pancreas triggers oxidative stress (Figure 3C). Interestingly, Perls' staining reveals preferential iron accumulation in the exocrine pancreas, sparing the islets of Langerhans (Figure S3A, top) that seem to function properly, as evidenced by normal oral glucose and insulin tolerance tests (Figure S3B). Iron loading of the exocrine pancreas without impact on glucose homeostasis has been reported for other mouse models of HH associated with absent or low hepcidin, such as *Hamp*$^{-/-}$ and *Hjv*$^{-/-}$ mice (Huang et al., 2005; Ramey et al., 2007). However, *Slc40a1*$^{C326S/C326S}$ animals differ from those HH models by clear signs indicating exocrine pancreatic failure. Indeed, hematoxylin and eosin staining demonstrates degeneration of the pancreatic acini starting at 21 weeks of age (Figure S3D) and worsening thereafter, with severe tissue degeneration in 7-month-old animals (Figure 3D). At 10 months of age, the degeneration becomes dramatic even though no signs of fibrosis were observed (Figure S3A, bottom). Consistent with a severely damaged exocrine pancreas, *Slc40a1*$^{C326S/C326S}$ mice show markedly reduced levels of lytic pancreatic enzymes such as amylase and elastase (Figure 3F). Increased plasma levels of pancreatic lipase (Figure 3E) further document the loss of integrity of the exocrine pancreas.

To understand why iron accumulates preferentially in the exocrine pancreas, we analyzed iron trafficking proteins by immunohistochemistry. Interestingly, TfR1 and DMT1 are predominantly detected in the endocrine pancreas of wild-type mice, and their expression is strongly reduced in *Slc40a1*$^{C326S/C326S}$ animals (Figure S3C). Hence, the severe iron accumulation in the exocrine pancreas of *Slc40a1*$^{C326S/C326S}$ mice cannot be explained by DMT1 and TFR1 overexpression and could plausibly be due to increased uptake of nontransferrin bound iron, e.g., via ZIP14, which is expressed on the plasma membrane of acinar cells of rats and is upregulated in response to iron overload (Nam et al., 2013). Importantly, FPN is detected in the endocrine pancreas of wild-type animals, and its expression persists in C326S mutant mice (Figure S3C). This finding provides a possible explanation for why the islets of Langerhans are iron spared and glucose homeostasis is unaltered. Notably, FPN is also detected on the surface of a restricted number of acinar cells (Figure S3C) in *Slc40a1*$^{C326S/C326S}$ mice, suggesting that those cells that lack Fpn expression may be prone to iron accumulation and oxidative stress and destined for degeneration. However, it remains unclear what drives FPN expression in some acinar cells and not others.

Figure 2. Analysis of Spleen and Duodenum

(A) Splenic nonheme iron was measured in 8- and 24-week-old mice.

(B) Perls' staining showing iron depletion in macrophages of the red pulp (RP) in the spleen of 24-week-old *Slc40a1*$^{C326S/C326S}$ male mice.

(C) Western blot analysis of FPN and ferritin light chain (FTL) expression in the spleen of 24-week-old animals. β-actin (ACTB) was used as loading control.

(D) Perls' staining (top) showing low iron levels in the duodenum of 24-week-old *Slc40a1*$^{C326S/C326S}$ male mice; IHC analyses showing high amounts of FPN (middle) and DMT1 (bottom) at the basolateral and apical membrane of enterocytes.

(E) Western blot analysis of DMT1 and FPN protein expression in the duodenum at 24 weeks of age. Mouse genotype is indicated. β-actin (ACTB) ascertained equal sample loading.

(F–I) qRT-PCR analysis of Fpn (F), DMT1-1A (G), DMT1-IRE (H), and Dcytb (I) mRNA in the duodenum of 24-week-old mice.

Data are reported as mean ± SEM. Student's t test: *p < 0.05; **p < 0.01; ***p < 0.001; ****p < 0.0001. See also Figure S2.

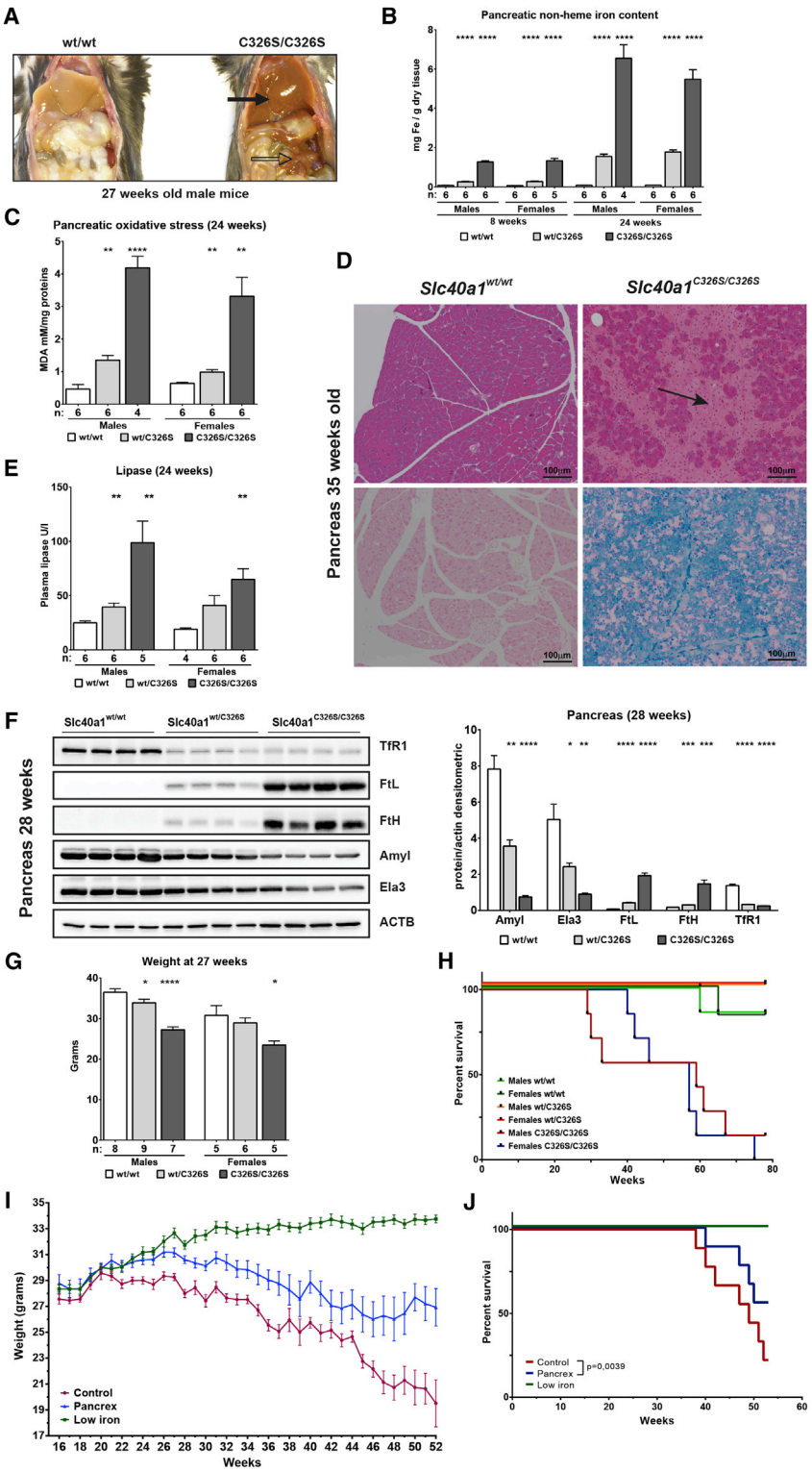

Figure 3. Systemic Iron Overload Causes Fatal Pancreatic Failure in C326S FPN Mutant Mice

(A) Macroscopical analysis showing strong brown coloration of the liver (plain arrow) and pancreas (empty arrow) of 27-week-old *Slc40a1*$^{C326S/C326S}$ mice, suggestive of iron deposition.

(B) Nonheme iron levels in the pancreas of wild-type and C326S FPN mutant mice at 8 or 24 weeks of age.

(C) TBARS assay showing increased lipid peroxidation and thus oxidative stress in pancreas of 24-week-old mice; TBARS levels were normalized against total protein content.

(D) Hematoxylin and eosin (H&E, top) and Prussian blue iron (bottom) staining of pancreatic sections from 35-week-old mice; the light purple color (black arrow) in H&E stained sections of mutant mice shows the degeneration of acinar cells.

(E) Plasma levels of pancreatic lipase in 24-week-old mice.

(F) Western blot analysis of TFR1, ferritin light (FTL) and heavy (FTH) chain, amylase (Amyl), and pancreatic elastase (Ela3) expression in the pancreas of wild-type, heterozygous, and homozygous C326S FPN mutant mice at 28 weeks of age; β-actin (ACTB) has been used as loading control. The western blot signals were quantified, and the results are shown as histograms.

(G) Body weight at 27 weeks of age.

(H) Kaplan-Meier survival curve showing premature death in *Slc40a1*$^{C326S/C326S}$ homozygous mice.

(I) *Slc40a1*$^{C326S/C326S}$ male mice (16 weeks old) were maintained on a control (200 ppm iron) versus low-iron diet (<10 ppm iron), or on a control diet supplemented with the Pancrex preparation. Body weight was determined weekly and reported.

(J) Kaplan-Meier survival curve of mice subjected to different dietary treatments as indicated in (I). Log rank Mantel-Cox test p value is indicated.

Data are reported as mean ± SEM. Student's t test: *p < 0.05; **p < 0.01; ***p < 0.001; ****p < 0.0001. See also Figure S3.

Surprisingly, while *Slc40a1*$^{C326S/C326S}$ mice appear overall healthy in early adulthood, both male and female C326S FPN mutant animals display a substantial wasting at 27 weeks of age (Figure 3G). This weight loss could be explained by malabsorption as a result of insufficient production of digestive enzymes by the failing exocrine pancreas (see below). In sharp contrast with the previously reported mouse models with systemic iron overload, *Slc40a1*$^{C326S/C326S}$ animals have a shorter lifespan than control littermates and start to die from 7 months of age (Figure 3H). Death is preceded by a sudden and profound loss of body weight down to 17–20 g, with mice humping the back and manifesting clear signs of sickness. Hence, FPN resistance to hepcidin is lethal in mice.

Compared to *Slc40a1*$^{C326S/C326S}$ animals, *Slc40a1*$^{wt/C326S}$ mice exhibit overall a much weaker pancreatic phenotype, with less iron accumulation (Figure 3B), less oxidative stress (Figure 3C), reduced plasma lipase levels (Figure 3E), and a minor decrease in amylase and elastase (Figure 3F). These milder

alterations do not cause the pathologies observed in *Slc40a1*$^{C326S/C326S}$ mice and allow for a normal lifespan (Figure 3H). Notably, exocrine pancreatic failure was also not reported for patients with HH type 4, who carry heterozygous FPN gain-of-function mutations.

To directly test the hypothesis that body weight loss and premature death of FPN C326S homozygous mutant animals are due to iron overload, *Slc40a1*$^{C326S/C326S}$ mice were maintained on an iron-deficient (<10 ppm iron) versus standard diet (~200 ppm iron) starting from 16 weeks of age. As shown in Figures 3I and 3J, the low-iron diet completely prevents the body weight loss and restores survival. These findings demonstrate that *Slc40a1*$^{C326S/C326S}$ mice indeed succumb to iron overload.

To further test whether exocrine pancreatic failure is a leading cause of wasting and death, the standard chow was supplemented with Pancrex, a compound commonly used clinically in pancreatic enzyme replacement therapy (PERT) (Fieker et al., 2011). PERT significantly ameliorated the condition of *Slc40A1*$^{C326S/C326S}$ mice, with partial reversion of body weight loss (Figure 3I) and improved survival (Figure 3J). Iron overloading and failure of the exocrine pancreas thus contribute to the weight loss and premature lethality of *Slc40a1*$^{C326S/C326S}$ mice. While the effect of Pancrex is obvious, it is not complete. The partial effectiveness could result from a still suboptimal PERT protocol but is likely also due to the mode of action of Pancrex, which corrects only some of the digestive consequences of pancreatic degeneration but leaves the mice with a severely damaged organ. Furthermore, additional yet-unidentified factors could also contribute to mouse wasting and death.

Our study shows that a single C326S substitution in FPN causes resistance to hepcidin in vivo and ex vivo, recapitulating key features of human HH type 4. It also uncovers the critical importance of the hepcidin-FPN regulatory circuitry for organismal survival. In contrast to previously reported mouse models of dietary systemic iron overload, the C326S FPN line shows shortened lifespan.

The absence of a hormone or the disruption of binding to its receptor could in principle yield identical phenotypes. FPN C326S mice and Hamp$^{-/-}$ animals display similar phenotypic abnormalities, such as iron accumulation in liver, pancreas, and kidney, and iron depletion in duodenum and spleen (Lesbordes-Brion et al., 2006; Moulouel et al., 2013). However, Hamp$^{-/-}$ mice notably have not been reported to die prematurely and hence do not phenocopy C326S FPN mutant animals completely. This difference suggests that additional functions of hepcidin, modes of regulation of FPN, and/or genetic modifiers of iron-mediated lethality are to be discovered.

EXPERIMENTAL PROCEDURES

Mice

Unless specified, all mice analyzed were on a mixed 129P2/C57BL6 genetic background, and wild-type littermates were used as controls. Mice were housed in the EMBL animal facility under a constant light-dark cycle and maintained on a standard mouse diet containing 200 ppm iron (Teklad 2018S, Harlan) with ad libitum access to food and water. Custom low-iron (E15510-24), control (E15510-24 supplemented with 200 ppm iron), and Pancrex (E15510-24 supplemented with 200 ppm iron and 10 g/kg Pancrex) chows were obtained from SSNIFF GmbH and given to B6N8F2 mice. Heparinized blood was collected by cardiac puncture from mice euthanized by CO_2 inhalation. For molecular analyses, mice were sacrificed by cervical dislocation to avoid proteome degradation. All mouse breeding and animal experiments were approved by and conducted in compliance with the guidelines of the EMBL Institutional Animal Care and Use Committee.

Isolation of BMDM and Hepcidin Treatment

Bone marrow cells were flushed from tibia and femur using ice-cold Hank's balanced salt solution (HBSS) and filtered through a 70 μm cell strainer. Cells were seeded at a density of 350,000 cells/cm^2 in RPMI1640-Glutamax medium (Life Technologies) supplemented with 10% of heat-inactivated fetal bovine serum (Thermo), 1% penicillin/streptomycin (Sigma), and 10 ng/ml M-CSF1 (Sigma). After 4 days, nonadherent cells were removed by HBSS washing, and the medium was replaced daily until cell harvesting (typically 6–7 days after seeding). Hepcidin treatment was performed as indicated using synthetic hepcidin 25 (Peptides International).

Hematology, Plasma Biochemistry, and Tissue Iron Quantification

Hematological parameters were determined using the ABC ScilVet analyzer (ABX Diagnostics). Plasma iron concentrations and unsaturated iron binding capacity were assessed using the SFBC and UIBC kits (Biolabo). Transferrin saturation was calculated using the formula SFBC / (SFBC + UIBC) × 100. Plasma ferritin measurements were performed using an Olympus AU400 analyzer at the Claude Bernard Institute (Paris, France). Plasma lipase, GOT, GTP, urea, creatinine, Na, K, and P were measured with a Hitachi 917E analyzer. Plasma Zn and Cu were measured by ICP/MS. Tissue nonheme iron content was measured using the bathophenanthroline method and calculated against dry weight tissue (Torrance and Bothwell, 1968).

Isolation of BMDMs and Hepcidin Treatment

Bone marrow cells were flushed from tibia and femur using ice-cold HBSS and filtered through a 70 μm cell strainer. Cells were seeded at a density of 350,000 cells/cm^2 in RPMI1640-Glutamax medium (Life Technologies) supplemented with 10% of heat-inactivated FBS (Thermo), 1% penicillin/streptomycin (Sigma), and 10 ng/ml M-CSF1 (Sigma). After 4 days, nonadherent cells were removed by HBSS washing, and the medium was replaced daily until cell harvesting (typically 6–7 days after seeding). Hepcidin treatment was performed as indicated using synthetic hepcidin 25 (Peptides International).

Immunohistochemistry

Tissues obtained from adult mice were fixed for 24 hr in 10% neutral buffered formalin (Sigma), dehydrated, and paraffin embedded. Tissue sections (4 μm) were mounted on Polysine slides (Thermo Scientific), rehydrated, and treated for 10 min with 3% H_2O_2 (Sigma) to block the endogenous peroxidases. After washing in distilled water, tissue slides were subjected to microwave-mediated antigen retrieval using the Citraplus reagent (Biogenex). After 40 min of cooling, slides were washed three times in PBS and subjected to immunorecognition using the Vectastain ABC mouse and rabbit kits (Vector Labs) following manufacturer's instructions. Antibody dilution and catalog number are reported in the Supplemental Experimental Procedures. Tissue slides have been developed using the Vector AEC substrate (Vector labs), rinsed with distilled water, counterstained with hematoxylin, washed in PBS, and mounted using the VectaMount AQ mounting medium (Vector Labs).

Western Blotting

Protein lysates were obtained by homogenizing snap-frozen tissues in RIPA buffer supplemented with protease inhibitors (Roche) as described (Galy et al., 2004). Protein concentration was determined using the DC protein assay (BioRad). Total protein (50 μg) was subjected to western blot analysis with the antibodies listed in the Supplemental Experimental Procedures. Western blot images were acquired and quantified with the Vilber Lourmat Fusion-FX system and normalized to β-actin (ACTB).

RNA Extraction, Reverse Transcription, and qRT-PCR

Total RNA was isolated using TRIzol (Life Technologies), reverse transcribed, and used in SYBR green qPCR, as described (Altamura et al., 2010). mRNA expression was calculated relative to β-actin, and data were analyzed using the ΔΔCt method (Livak and Schmittgen, 2001). The primers used are listed in the Supplemental Experimental Procedures.

Statistical Analyses

Data are shown as mean ± SEM, and the number of mice (n) is indicated. Statistical analyses were performed using Prism v.6 (GraphPad). Two-tailed Student's t test p value was calculated against sex-matched wild-type mice. *p < 0.05, **p < 0.01, ***p < 0.001, and ****p < 0.0001 are indicated.

SUPPLEMENTAL INFORMATION

Supplemental Information includes Supplemental Experimental Procedures, three figures, and two tables and can be found with this article online at http://dx.doi.org/10.1016/j.cmet.2014.07.007.

ACKNOWLEDGMENTS

We are grateful to Martin Schneider, Oliver Strobel (University of Heidelberg), and Ellen Kienzle (University of Munich) for support in the pancreatic study. We thank Milene da Silva for the duodenal immunohistochemistry (IHC), Dunja Ferring-Appel for technical assistance, and the staff of the EMBL LAR for the animal care. M.U.M. acknowledges support of the Dietmar Hopp Stiftung. M.U.M. and M.W.H. acknowledge the Virtual Liver funding initiative of the BMBF. S.A. is supported by the Medical Faculty Heidelberg, the "Excellenzinitiative II" of the University of Heidelberg and the SFB1118.

Received: February 28, 2014
Revised: May 13, 2014
Accepted: July 7, 2014
Published: August 5, 2014

REFERENCES

Altamura, S., and Muckenthaler, M.U. (2009). Iron toxicity in diseases of aging: Alzheimer's disease, Parkinson's disease and atherosclerosis. J. Alzheimers Dis. *16*, 879–895.

Altamura, S., D'Alessio, F., Selle, B., and Muckenthaler, M.U. (2010). A novel TMPRSS6 mutation that prevents protease auto-activation causes IRIDA. Biochem. J. *431*, 363–371.

Brasse-Lagnel, C., Karim, Z., Letteron, P., Bekri, S., Bado, A., and Beaumont, C. (2011). Intestinal DMT1 cotransporter is down-regulated by hepcidin via proteasome internalization and degradation. Gastroenterology *140*, 1261–1271, e1.

Chung, J., Haile, D.J., and Wessling-Resnick, M. (2004). Copper-induced ferroportin-1 expression in J774 macrophages is associated with increased iron efflux. Proc. Natl. Acad. Sci. USA *101*, 2700–2705.

Donovan, A., Brownlie, A., Zhou, Y., Shepard, J., Pratt, S.J., Moynihan, J., Paw, B.H., Drejer, A., Barut, B., Zapata, A., et al. (2000). Positional cloning of zebrafish ferroportin1 identifies a conserved vertebrate iron exporter. Nature *403*, 776–781.

Donovan, A., Lima, C.A., Pinkus, J.L., Pinkus, G.S., Zon, L.I., Robine, S., and Andrews, N.C. (2005). The iron exporter ferroportin/Slc40a1 is essential for iron homeostasis. Cell Metab. *1*, 191–200.

Fernandes, A., Preza, G.C., Phung, Y., De Domenico, I., Kaplan, J., Ganz, T., and Nemeth, E. (2009). The molecular basis of hepcidin-resistant hereditary hemochromatosis. Blood *114*, 437–443.

Fieker, A., Philpott, J., and Armand, M. (2011). Enzyme replacement therapy for pancreatic insufficiency: present and future. Clin Exp Gastroenterol *4*, 55–73.

Galy, B., Ferring, D., Benesova, M., Benes, V., and Hentze, M.W. (2004). Targeted mutagenesis of the murine IRP1 and IRP2 genes reveals context-dependent RNA processing differences in vivo. RNA *10*, 1019–1025.

Galy, B., Ferring-Appel, D., Becker, C., Gretz, N., Gröne, H.J., Schümann, K., and Hentze, M.W. (2013). Iron regulatory proteins control a mucosal block to intestinal iron absorption. Cell Rep *3*, 844–857.

Hentze, M.W., and Kühn, L.C. (1996). Molecular control of vertebrate iron metabolism: mRNA-based regulatory circuits operated by iron, nitric oxide, and oxidative stress. Proc. Natl. Acad. Sci. USA *93*, 8175–8182.

Hentze, M.W., Muckenthaler, M.U., Galy, B., and Camaschella, C. (2010). Two to tango: regulation of Mammalian iron metabolism. Cell *142*, 24–38.

Huang, F.W., Pinkus, J.L., Pinkus, G.S., Fleming, M.D., and Andrews, N.C. (2005). A mouse model of juvenile hemochromatosis. J. Clin. Invest. *115*, 2187–2191.

Lesbordes-Brion, J.C., Viatte, L., Bennoun, M., Lou, D.Q., Ramey, G., Houbron, C., Hamard, G., Kahn, A., and Vaulont, S. (2006). Targeted disruption of the hepcidin 1 gene results in severe hemochromatosis. Blood *108*, 1402–1405.

Livak, K.J., and Schmittgen, T.D. (2001). Analysis of relative gene expression data using real-time quantitative PCR and the 2(-Delta Delta C(T)) Method. Methods *25*, 402–408.

Mastrogiannaki, M., Matak, P., Keith, B., Simon, M.C., Vaulont, S., and Peyssonnaux, C. (2009). HIF-2alpha, but not HIF-1alpha, promotes iron absorption in mice. J. Clin. Invest. *119*, 1159–1166.

McKie, A.T., Marciani, P., Rolfs, A., Brennan, K., Wehr, K., Barrow, D., Miret, S., Bomford, A., Peters, T.J., Farzaneh, F., et al. (2000). A novel duodenal iron-regulated transporter, IREG1, implicated in the basolateral transfer of iron to the circulation. Mol. Cell *5*, 299–309.

McLaren, C.E., Barton, J.C., Gordeuk, V.R., Wu, L., Adams, P.C., Reboussin, D.M., Speechley, M., Chang, H., Acton, R.T., Harris, E.L., et al.; Hemochromatosis and Iron Overload Screening Study Research Investigators (2007). Determinants and characteristics of mean corpuscular volume and hemoglobin concentration in white HFE C282Y homozygotes in the hemochromatosis and iron overload screening study. Am. J. Hematol. *82*, 898–905.

Moulouel, B., Houamel, D., Delaby, C., Tchernitchko, D., Vaulont, S., Letteron, P., Thibaudeau, O., Puy, H., Gouya, L., Beaumont, C., and Karim, Z. (2013). Hepcidin regulates intrarenal iron handling at the distal nephron. Kidney Int. *84*, 756–766.

Nam, H., Wang, C.Y., Zhang, L., Zhang, W., Hojyo, S., Fukada, T., and Knutson, M.D. (2013). ZIP14 and DMT1 in the liver, pancreas, and heart are differentially regulated by iron deficiency and overload: implications for tissue iron uptake in iron-related disorders. Haematologica *98*, 1049–1057.

Nemeth, E., Tuttle, M.S., Powelson, J., Vaughn, M.B., Donovan, A., Ward, D.M., Ganz, T., and Kaplan, J. (2004). Hepcidin regulates cellular iron efflux by binding to ferroportin and inducing its internalization. Science *306*, 2090–2093.

Pietrangelo, A. (2004). The ferroportin disease. Blood Cells Mol. Dis. *32*, 131–138.

Pietrangelo, A. (2010). Hereditary hemochromatosis: pathogenesis, diagnosis, and treatment. Gastroenterology *139*, 393–408, e1–e2.

Qiao, B., Sugianto, P., Fung, E., Del-Castillo-Rueda, A., Moran-Jimenez, M.J., Ganz, T., and Nemeth, E. (2012). Hepcidin-induced endocytosis of ferroportin is dependent on ferroportin ubiquitination. Cell Metab. *15*, 918–924.

Ramey, G., Faye, A., Durel, B., Viollet, B., and Vaulont, S. (2007). Iron overload in Hepc1(-/-) mice is not impairing glucose homeostasis. FEBS Lett. *581*, 1053–1057.

Sham, R.L., Phatak, P.D., West, C., Lee, P., Andrews, C., and Beutler, E. (2005). Autosomal dominant hereditary hemochromatosis associated with a novel ferroportin mutation and unique clinical features. Blood Cells Mol. Dis. *34*, 157–161.

Sham, R.L., Phatak, P.D., Nemeth, E., and Ganz, T. (2009). Hereditary hemochromatosis due to resistance to hepcidin: high hepcidin concentrations in a family with C326S ferroportin mutation. Blood *114*, 493–494.

Tang, S.H., Silva, F.J., Tsark, W.M., and Mann, J.R. (2002). A Cre/loxP-deleter transgenic line in mouse strain 129S1/SvImJ. Genesis *32*, 199–202.

Taylor, M., Qu, A., Anderson, E.R., Matsubara, T., Martin, A., Gonzalez, F.J., and Shah, Y.M. (2011). Hypoxia-inducible factor-2α mediates the adaptive increase of intestinal ferroportin during iron deficiency in mice. Gastroenterology *140*, 2044–2055.

Torrance, J.D., and Bothwell, T.H. (1968). A simple technique for measuring storage iron concentrations in formalinised liver samples. S. Afr. J. Med. Sci. *33*, 9–11.

Troadec, M.B., Ward, D.M., Lo, E., Kaplan, J., and De Domenico, I. (2010). Induction of FPN1 transcription by MTF-1 reveals a role for ferroportin in transition metal efflux. Blood *116*, 4657–4664.